Real-time hybrid simulation in the Pseudo-Dynamic Testing Facility at the Indian Institute of Technology Kanpur

Hironmoy Kakoty[1], Chinmoy Kolay[1,*], Shubham Raj[1] and Kamal K. Kar[2]

[1]Department of Civil Engineering, and
[2]Department of Mechanical Engineering and Material Science Programme, Indian Institute of Technology Kanpur, Kanpur 208 016, India

Real-time hybrid simulation (RTHS) is a state-of-the-art, accurate, affordable method for simulating seismic effects on structures with loading rate-dependent behaviour. In RTHS, a part of the system that cannot be accurately modelled numerically is simulated experimentally in the laboratory, and the rest numerically. The response of the hybrid system is obtained in real-time by solving the governing equations of motion. This communication demonstrates an implementation of RTHS in the Pseudo Dynamic Testing Facility at IIT Kanpur and its application to seismic response simulation of a two-storey reinforced concrete special moment-resisting frame building with in-house-built nonlinear viscoelastic dampers.

Keywords: Adaptive time series compensator, earthquake response, numerical damping, real-time hybrid simulation, viscoelastic damper.

HYBRID simulation (HS) and real-time hybrid simulation (RTHS) are efficient and well-accepted alternatives to the expensive shake table testing method for simulating seismic effects on structures. In the former, the simulation is performed in an extended timescale and used for structures with loading rate-independent behaviour. In the latter, the simulation is performed in real time (i.e. actual time scale) to simulate the system response with experimentally modelled rate-dependent components and devices. The two methods are increasingly becoming popular not only in the field of earthquake engineering but also in other fields, e.g. structural fire and wind engineering. Several research laboratories in the US, Japan, Canada, Italy, South Korea, Taiwan and China have implemented and employed the HS and RTHS techniques to study earthquake engineering problems. However, the application of such powerful tools has been limited in structural engineering research in India. To our knowledge, the RTHS technique has not been implemented yet in any research laboratories in India. Nevertheless, we have recently implemented and performed HS and RTHS in the Pseudo-Dynamic Testing Facility (PDTF) at the Indian Institute of Technology Kanpur (IITK), a unique facility in the country for seismic testing of prototypical structures[1]. It may be noted that conventional pseudo-dynamic tests have already been conducted in this facility, where the inertia and damping forces were modelled numerically[2,3]. In this study, the PDTF capabilities are upgraded to perform HS and RTHS using a MATLAB/Simulink-based finite element (FE) program and parametrically dissipative explicit unconditionally stable direct integration algorithms. This communication discusses some key aspects of RTHS implementation and its application to seismic response simulation of a two-storey reinforced concrete (RC) special moment-resisting frame (SMRF) building with nonlinear viscoelastic dampers.

Figure 1 demonstrates the concept of an RTHS considering a two-storey RC-SMRF with two nonlinear viscoelastic dampers. As shown in the figure, the two dampers were modelled physically in the laboratory (i.e. experimental substructures) because they are generally difficult to model numerically due to their response being dependent on the amplitude and rate of the applied strain and the ambient temperature. Note that in some simulations, only one damper in the second storey was used, as described later. The remaining system (i.e. RC-SMRF, braces, seismic floor masses and inherent damping) was modelled numerically (i.e. analytical substructure), where the P–Δ effects were included through a lean-on column. The numerically modelled seismic floor masses were 42.1 and 41.9 t for the first and second floors respectively. The inherent damping was modelled using a mass and current tangent stiffness proportional damping matrix, where the proportionality constants were determined to assign 2% damping to the first and second natural vibration modes. The prototype RC-SMRF was adopted from Kolay and Ricles[4]. The response of the hybrid system subjected to seismic ground excitation can be determined by solving the following semi-discrete equations of motion in real time:

$$\mathbf{M}\ddot{\mathbf{X}}_{n+1} + \mathbf{C}\dot{\mathbf{X}}_{n+1} + \mathbf{R}^{\mathrm{a}}_{n+1} + \mathbf{R}^{\mathrm{e}}_{n+1} = \mathbf{F}_{n+1}, \tag{1}$$

where $\mathbf{M}$ and $\mathbf{C}$ are the numerically modelled mass and damping matrices respectively; $\mathbf{R}^{\mathrm{a}}$ and $\mathbf{R}^{\mathrm{e}}$ the restoring forces from the analytical and experimentally substructures respectively; $\mathbf{F}_{n+1}$ the vector of effective earthquake forces and n is the time step. This study uses the explicit, unconditionally stable and parametrically dissipative MKR-α method[5] to integrate the equations of motion. At each time step (n + 1), the displacement $\mathbf{X}_{n+1}$ and velocity $\dot{\mathbf{X}}_{n+1}$ are calculated explicitly based on the previous step response (i.e. $\mathbf{X}_n$, $\dot{\mathbf{X}}_n$ and $\ddot{\mathbf{X}}_n$). Note that the MKR-α method is a modified and improved version of the KR-α method[6], and both have been successfully used to perform RTHS[4,7–9]. Once $\mathbf{X}_{n+1}$ and $\dot{\mathbf{X}}_{n+1}$ are known, a state determination is performed to calculate the restoring forces $\mathbf{R}^{\mathrm{a}}_{n+1}$ for the analytical substructure. Simultaneously, the displacement or deformation commands corresponding to the experimental substructure DOFs are physically applied through servo-hydraulic actuators and the restoring forces are measured

*For correspondence. (e-mail: ckolay@iitk.ac.in)

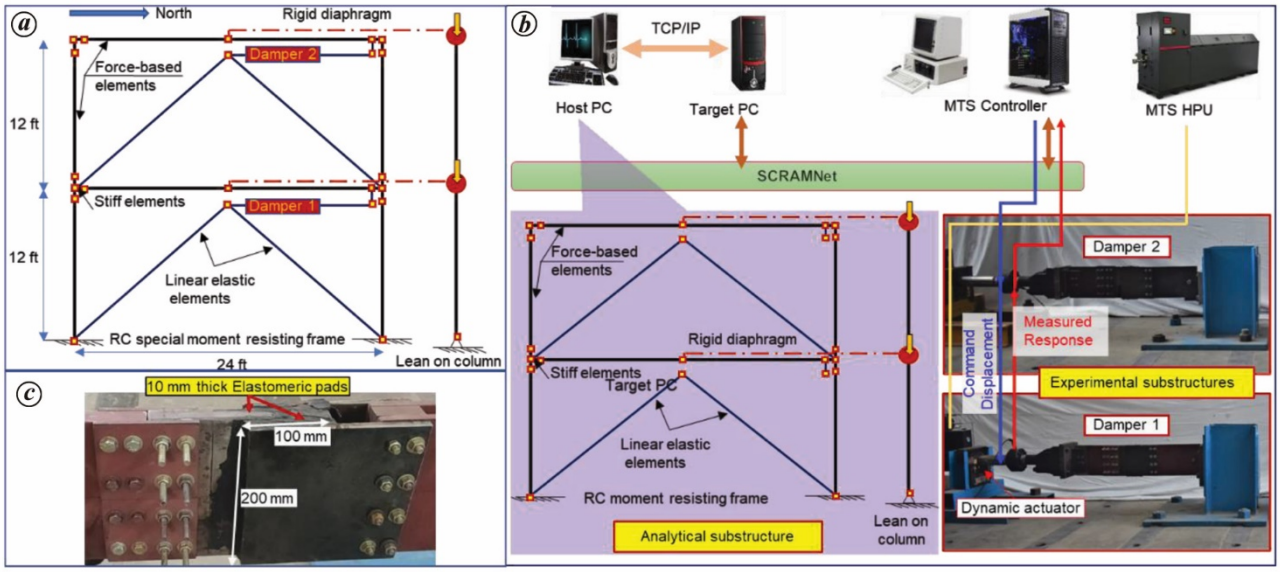

Figure 1. Concept of real-time hybrid simulation (RTHS): ***a***, Two-storey reinforced concrete (RC)-special moment resisting frame (SMRF) prototype frame fitted with VE dampers. ***b***, RTHS framework showing the substructured hybrid system with its key components. ***c***, In-house-built viscoelastic damper (1 ft = 0.3048 m).

using load cells, which leads to $\mathbf{R}^{e}_{n+1}$. Then, the equations of motion are solved to determine the current accelerations $\ddot{\mathbf{X}}_{n+1}$, and this process is repeated for the subsequent time steps. Note that the MKR-α method employs a set of weighted equations of motion instead of eq. (1) to introduce controllable numerical damping. These equations are not presented here to keep the discussion brief and focused.

The above process of numerical integration and state determination is performed in a Simulink model[8] developed in HybridFEM-MH[10], a MATLAB and Simulink-based[11] finite element program. This model is configured and compiled in a Windows-based PC, called the host PC (Figure 1 *b*). Before running an RTHS, the compiled model is downloaded to the target PC (Speedgoat real-time target machine SN5353 fitted with the seventh generation Intel core i7 4.2 GHz CPU) that runs the model using MathWorks Simulink Real Time environment[12]. At each time step, the target PC generates the target displacement commands for the experimental substructures by solving the equations of motion in real-time. These commands are sent to the servo-controller (MTS FT-60) over a shared common random access memory-based network (SCRAMNet GT200) after necessary modification, which is discussed later. These displacements are imposed on the experimental substructures using dynamic actuators (two 100 kN MTS DuraGlide 244G2 actuators), and the restoring forces and displacements from the experimental substructures are measured and recorded in the controller. These measured responses are made available to the target PC through SCRAMNet to calculate displacement commands for the next step. Figure 1 *b* presents a schematic of the interaction of the software and hardware components used in the RTHS framework.

Each damper (i.e. experimental substructure) used in this study consists of two 10 mm thick viscoelastic pads (100 × 200 mm) sandwiched between three mild steel (MS) plates. Figure 1 *c* provides a close-up view of one of the dampers. The middle MS plate (200 × 200 × 20 mm) is connected to the actuator at one end, and the outer MS plates (200 × 200 × 10 mm each) to the support at the other end using connecting plates (Figure 1 *b*). The damper end connections are such that the device has a stroke of ±40 mm, which corresponds to 400% shear strain in the viscoelastic pads. The formulation of the viscoelastic pads used in this study consists of Indian natural rubber (100 g), zinc oxide (5 g), stearic acid (2 g), TDQ (2 g), CBS (0.8 g), TMT (0.2 g), sulphur (2.5 g), carbon black (35 g) and processing oil (3.5 g). Currently, work is underway at IITK to optimize the above formulation and improve the characteristics of the damper. The equivalent stiffness and damping coefficients of the experimental substructures need to be determined for use in the model-based integration parameters of the MKR-α method to retain the unconditional stability of the method. Therefore, the dampers were characterized by applying sinusoidal displacement cycles of varying amplitudes (5–15 mm) and frequencies (0.1–3 Hz), as shown in Figure 2 for one of the dampers. Then, a Kelvin–Voigt model (i.e. a spring and dashpot in parallel) was fitted to the force deformation behaviour obtained from each test. Considering all the tests, the maximum stiffness and damping coefficients were taken to be their corresponding equivalent values.

In what follows, three key aspects of RTHS, namely (i) an accurate actuator control, (ii) the need for controllable numerical damping, and (iii) an advanced analytical modelling approach, are discussed. For the first two aspects, the beams and columns of the analytical substructure were modelled using linear elastic beam–column elements. For the last aspect, they were modelled using nonlinear force-based

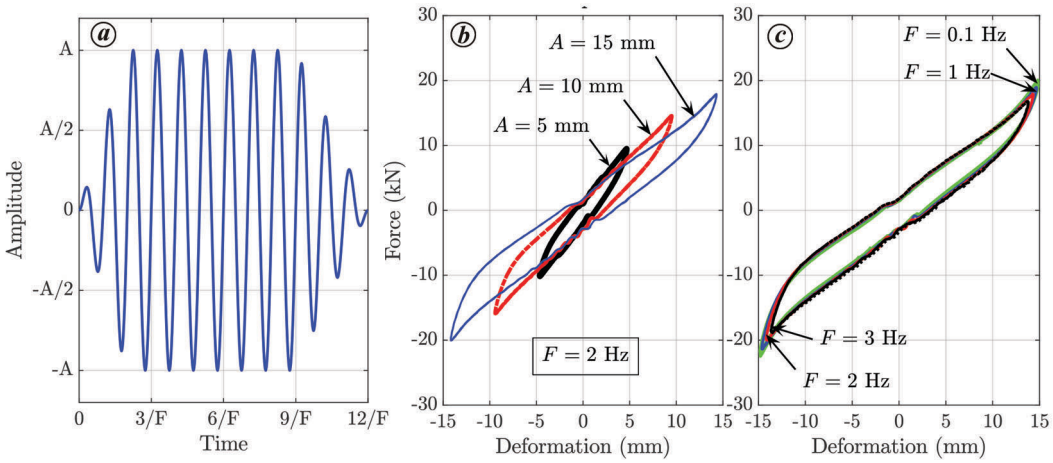

Figure 2. Damper characterization: ***a***, Loading protocol (where A and F are the amplitude and frequency of excitation respectively). ***b***, Damper force deformation at different amplitudes. ***c***, Damper force deformation at different frequencies.

Table 1. Test matrix for real-time hybrid simulation with objectives and relevant parameters

Test ID	Objectives	Analytical substructure	Damper in storey	ATS compensator	$(\rho_\infty)^2$	Salient results
1	Actuator control	Linear elastic	First and Second	No	0.25	Figure 3
2			Second	Yes $a_2 \in [0, 4 \times 10^{-4}]$ s^2		Figure 4
3				Yes $a_2 \in [0, 5 \times 10^{-5}]$ s^2		Figure 5
4				Yes Modified ATS $a_2 \in [0, 5 \times 10^{-5}]$ s^2		Figure 6, Figure 7
5			First and Second			Figure 3
6	Numerical damping		Second		0.50	Figure 7
7	Advanced modelling	Nonlinear model	First and Second		0.50	Figure 8

fibre elements with a fixed number of iterations[4]. Table 1 presents the RTHS test matrix used along with the objective of each test, relevant parameters and the figure numbers where the salient results are presented. All these tests used the LOS270 component of the 1994 Northridge earthquake record (PEER NGA Strong Motion Database). For the first six tests, the ground motion and the measured damper force were scaled by 0.3 and 12 respectively, where the latter scale factor indicates that the total shear area of the prototype dampers in a storey is 12 times that of the laboratory model. These were done to keep the damage in the viscoelastic material small so that the dampers could be used for several RTHS. Such scaling of the measured force is a unique feature offered by RTHS. On the other hand, for the last test, the ground motion was scaled to the design basis earthquake (DBE) level (Table 1), considering the building to be located in the Los Angeles area, USA, on a stiff soil site (design parameters $S_{DS} = 1.0$ g, $S_{D1} = 0.6$ g, $T_0 = 0.12$ s and $T_s = 0.6$ s)[13]. The scale factor (0.866) was calculated to minimize the sum of square error between the ground motion spectrum and the target design spectrum in the period range $0.2T_1$ to $1.5T_1$, where T_1 is the undamped fundamental period of the system. Furthermore, the dampers were assumed to be 1/3-scaled models of their prototypes. Hence, during the last RTHS, the computed damper deformations were scaled down by a factor of three. The measured restoring forces were scaled up by a factor of nine to satisfy the similitude requirements, where the time and stress scale factors were considered unity. All the simulations were performed using a time-step size of $\Delta t = 3\delta t$, where $\delta t =$ (1/1024) s is the sampling period of the servo-controller used in this study.

In an RTHS, the measured actuator displacements (or specimen deformations) always have some variable delay and amplitude error due to the combined dynamics of the servo-hydraulic system and experimental substructures. To demonstrate this, Figure 3 presents the target and measured responses (see the curves with no compensation) of the two actuators obtained from RTHS #1 (Table 1). The measured displacements have time-varying delays (the maximum is around 30 and 20 ms in actuators 1 and 2 respectively) and amplitude errors. A delay in the measured specimen displacement can impart negative damping into the hybrid system, making the response grow without bounds and leading to an unstable simulation. For the results presented in Figure 3, the test was stopped after 2 sec as the response (i.e. target and measured displacements with no compensation) started growing. The adaptive time series

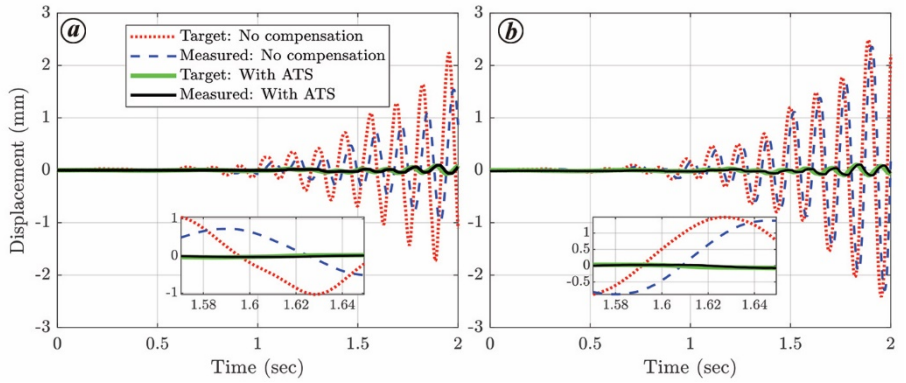

Figure 3. Comparison of target and measured actuator displacements with and without adaptive time series (ATS) compensator for (***a***) actuator 1 and (***b***) actuator 2.

(ATS) compensator developed by Chae *et al.*[14] was used in this study to compensate for the time-varying delay and amplitude error. As described below, the correct results (RTHS #5) (Table 1) obtained using the modified ATS compensator are also shown in Figure 3 (see the target and measured displacements with ATS).

For a given actuator, ATS modifies the target displacement signal to minimize the error between the target and the measured displacements as follows[14]

$$u_k^{\mathrm{c}} = a_{0k} x_k^{\mathrm{t}} + a_{1k} \dot{x}_k^{\mathrm{t}} + a_{2k} \ddot{x}_k^{\mathrm{t}}, \tag{2}$$

where u_k^{c} is the compensated or modified displacement sent to the servo-controller at time $t_k = k\delta t$; k is an integer and $x_k^{\mathrm{t}}, \dot{x}_k^{\mathrm{t}}$ and $\ddot{x}_k^{\mathrm{t}}$ are the target displacement, velocity and acceleration respectively. The parameters a_{0k}, a_{1k} and a_{2k} are calculated based on the measured displacement over the previous interval $q\delta t$ (= 1 s) using a least square approximation (eq. (3)) and updated continuously during the simulation.

$$\mathbf{A} = (\mathbf{X}_{\mathbf{m}}^{\mathbf{T}} \mathbf{X}_{\mathbf{m}})^{-1} \mathbf{X}_{\mathbf{m}}^{\mathbf{T}} \mathbf{U}^{\mathbf{c}}, \tag{3}$$

where $\mathbf{A} = [a_{0k}\ a_{1k}\ a_{2k}]^T$; $\mathbf{X}_{\mathbf{m}} = [\mathbf{x}^{\mathbf{m}}\ \dot{\mathbf{x}}^{\mathbf{m}}\ \ddot{\mathbf{x}}^{\mathbf{m}}]$; $\mathbf{x}^{\mathbf{m}} = [x_{k-1}^{\mathrm{m}} x_{k-2}^{\mathrm{m}} \cdots x_{k-q}^{\mathrm{m}}]^T$; $\mathbf{U}^{\mathbf{c}} = [u_{k-1}^{\mathrm{c}} u_{k-2}^{\mathrm{c}} \cdots u_{k-q}^{\mathrm{c}}]$, and x_{k-1}^{m} and u_{k-1}^{c} are the measured and compensated displacements respectively. At the beginning and end of an RTHS, the measured displacements x^{m} are generally small and may have significant high-frequency noise. During these stages, the parameters are calculated using eq. (3) may show sharp variation and make the RTHS unstable. Therefore, ATS is activated when the root mean square (RMS) of the measured displacement over a previous $q\delta t$ window exceeds a specified threshold (0.5 mm) and is deactivated when it falls below the threshold. During this initial stage, ATS runs with predefined constant parameters, which are calculated before an RTHS based on a band-limited white noise test[15]. When ATS is deactivated, the last set of values of the parameters is held constant till the end of the simulation. Several previous studies have shown that the ATS compensator works well[7–9,14]. However, the ATS compensator amplifies the higher frequencies in a target displacement signal, and the amplification magnitude increases with the ATS parameters[15]. This can be addressed by limiting the values of the parameters and their rates of change as proposed by Chae *et al.*[14]. Figure 4 *a* shows the time history of the compensated (u^{c}), target (x^{t}) and measured (x^{m}) displacements for damper-2 from an RTHS with the ATS compensator (i.e. RTHS #2) (Table 1). In this test, the limits used for the ATS parameters are as follows: $a_0 \in [0.70,\ 1.30]$, $a_1 \in [0,\ 0.04]$ s and $a_2 \in [0,\ 4 \times 10^{-4}]$ s^2. To quantify the actuator control accuracy, the normalized energy error (NEE) and normalized root mean square error (NRMSE) metrics are used as follows

$$\mathrm{NEE} = \left| \frac{\sum_{n=1}^{N} (x_n^{\mathrm{m}})^2 - \sum_{n=1}^{N} (x_n^{\mathrm{t}})^2}{\sum_{n=1}^{N} (x_n^{\mathrm{t}})^2} \right|, \tag{4}$$

$$\mathrm{NRMSE} = \frac{\sqrt{\frac{1}{N} \sum_{n=1}^{N} (x_n^{\mathrm{m}} - x_n^{\mathrm{t}})^2}}{\max(\mathbf{x}^{\mathrm{t}}) - \min(\mathbf{x}^{\mathrm{t}})}, \tag{5}$$

where $\mathbf{x}^{\mathrm{t}}$ and $\mathbf{x}^{\mathrm{m}}$ are the vectors of target and measured actuator displacements respectively, and N is the length of the vectors. Note that NEE and NRMSE are sensitive to amplitude error and delay respectively. The synchronization subspace plot between the measured and target displacements and the small NEE (0.86%) and NRMSE (0.20%) values in Figure 4 *b* indicates accurate actuator tracking, where a 45° line indicates perfect tracking. However, the amplification of higher frequencies (the compensated displacement u^{c} in Figure 4 *a*) cannot be ignored as it leads to an undesired damper force–deformation hysteresis response (Figure 4 *c*) contaminated by higher frequencies. Note that such higher frequencies are an artefact of the RTHS and

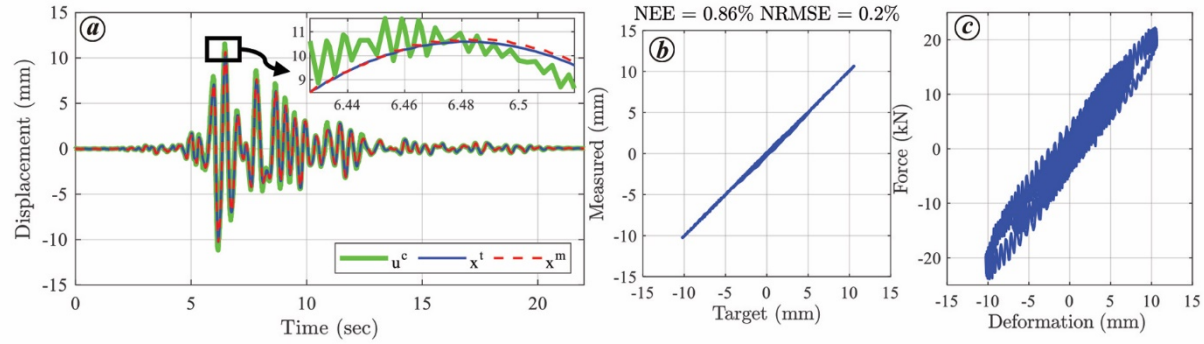

Figure 4. Effect of the ATS compensator on RTHS results: ***a***, Time histories of compensated (u^c), target (x^t) and measured (x^m) displacements for damper-2 showing amplification of higher frequencies in u^c. ***b***, Synchronization subspace plot. ***c***, Force deformation behaviour of the connected damper.

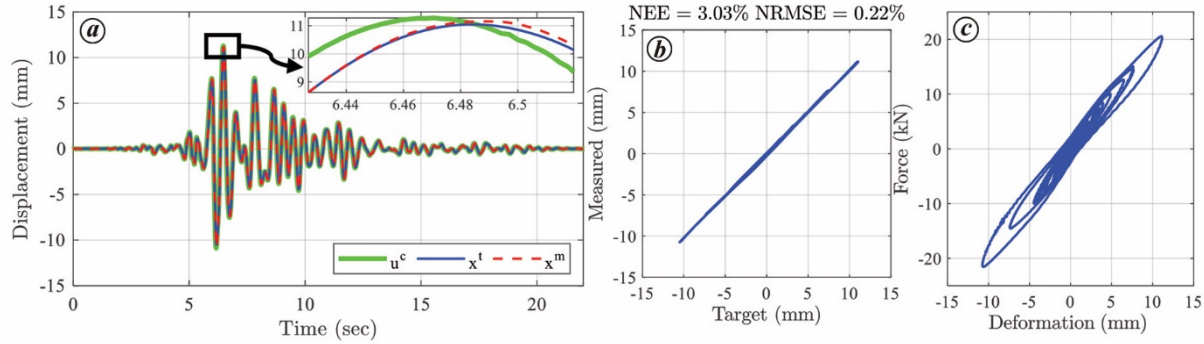

Figure 5. Effect of limit on ATS parameter a_2: ***a***, Time histories of compensated (u^c), target (x^t) and measured (x^m) displacements for damper-2. ***b***, Synchronization subspace plot. ***c***, Force deformation behaviour of the connected damper.

must be eliminated. Also, such high-frequency oscillations can often lead to an unstable test.

To eliminate such high-frequency oscillations, the same test (i.e. RTHS #2) was repeated by placing a tighter upper limit on a_2 as 5×10^{-5} s^2 (i.e. one-eighth of the previous limit). Figure 5 presents results from this RTHS (i.e. RTHS #3). The figure shows that the high-frequency oscillations are eliminated from the compensated signal, which is also apparent from the force–deformation hysteresis of the damper. However, this is achieved at the cost of an increased NEE (3.03%) and NRMSE (0.22%), which indicates a reduction in the actuator control accuracy. Note that a higher value of NEE implies a higher amplitude error in the actuator tracking displacement. Thus, it is a trade-off between eliminating high-frequency oscillations and accurate actuator control. Nevertheless, the accuracy of actuator control can be improved by recalculating parameters a_0 and a_1 when parameter a_2 reaches its maximum value of $\bar{a}_2$ as follows

$$\bar{\mathbf{A}} = (\bar{\mathbf{X}}_\mathbf{m}^\mathbf{T} \bar{\mathbf{X}}_\mathbf{m})^{-1} \bar{\mathbf{X}}_\mathbf{m}^\mathbf{T} \{\mathbf{U}^\mathbf{c} - \bar{a}_2 \ddot{\mathbf{x}}^\mathbf{m}\}, \tag{6}$$

where $\bar{\mathbf{A}} = [a_{0k} a_{1k}]^T$; $\bar{\mathbf{X}}_\mathbf{m} = [\mathbf{x}^\mathbf{m} \dot{\mathbf{x}}^\mathbf{m}]$ and $\ddot{\mathbf{x}}^\mathbf{m} = [\ddot{x}^m_{k-1} \ddot{x}^m_{k-2} \ldots \ddot{x}^m_{k-q}]^T$. Equation (6) was derived from the formulation of the ATS compensator by Chae *et al.*[14]. The same test (i.e. RTHS #3) was repeated (i.e. RTHS #4) using the modified ATS while keeping all other parameters constant. The results in Figure 6 show that the NEE value is reduced significantly (by a factor of ten), while the NRMSE value is comparable to the previous RTHS. Thus, the proposed modification to the ATS compensator seems promising for RTHS applications. Note that the limits on ATS parameters and the threshold value may vary depending on the hybrid system, servo-hydraulic system and numerical characteristics of the integration algorithm used for RTHS. Hence, some trial tests are required to tune the parameter limits.

Another issue in RTHS is that the measured restoring forces from experimental substructures often contain high-frequency noise, which can excite spurious higher modes in the numerical substructure and lead to incorrect simulation. The commonly available data-filtering techniques are inevitably associated with some delay and hence cannot be used in RTHS, as a delay in measured force leads to unstable simulation, as discussed earlier. The MKR-α method employed in this study provides controllable numerical damping using a single parameter ρ_∞. This controllable damping is useful in eliminating the effects of high-frequency noise from the experimental substructure. The user-defined parameter ρ_∞ denotes the high-frequency spectral radius of the amplification matrix of the algorithm and

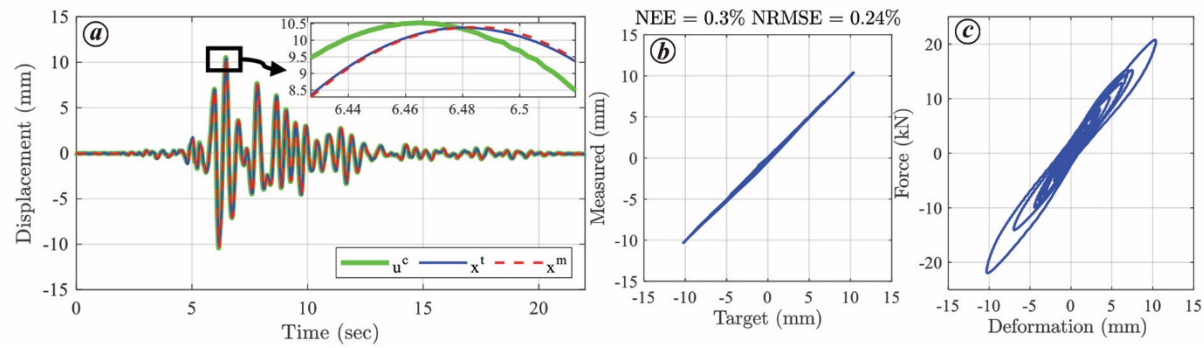

Figure 6. Results obtained using modified ATS: ***a***, Time histories of compensated (u^c), target (x^t) and measured (x^m) displacements for damper-2. ***b***, Synchronization subspace plot. ***c***, Force deformation behaviour of the connected damper.

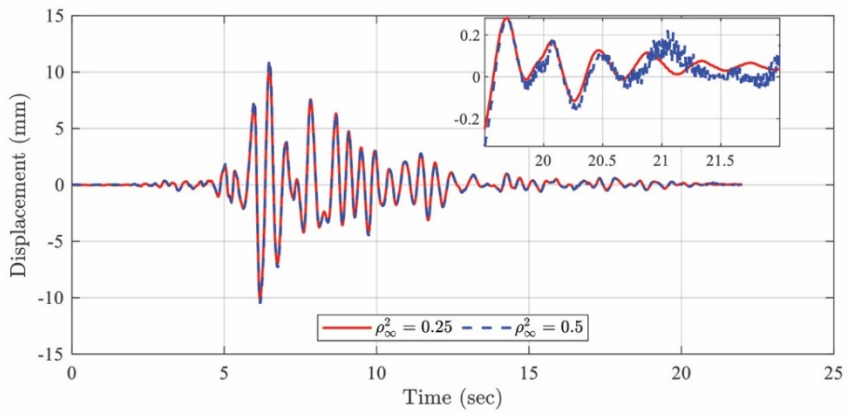

Figure 7. Time history of target damper displacements for $\rho_\infty^2 = 0.25$ and $\rho_\infty^2 = 0.5$ showing the efficacy of numerical damping.

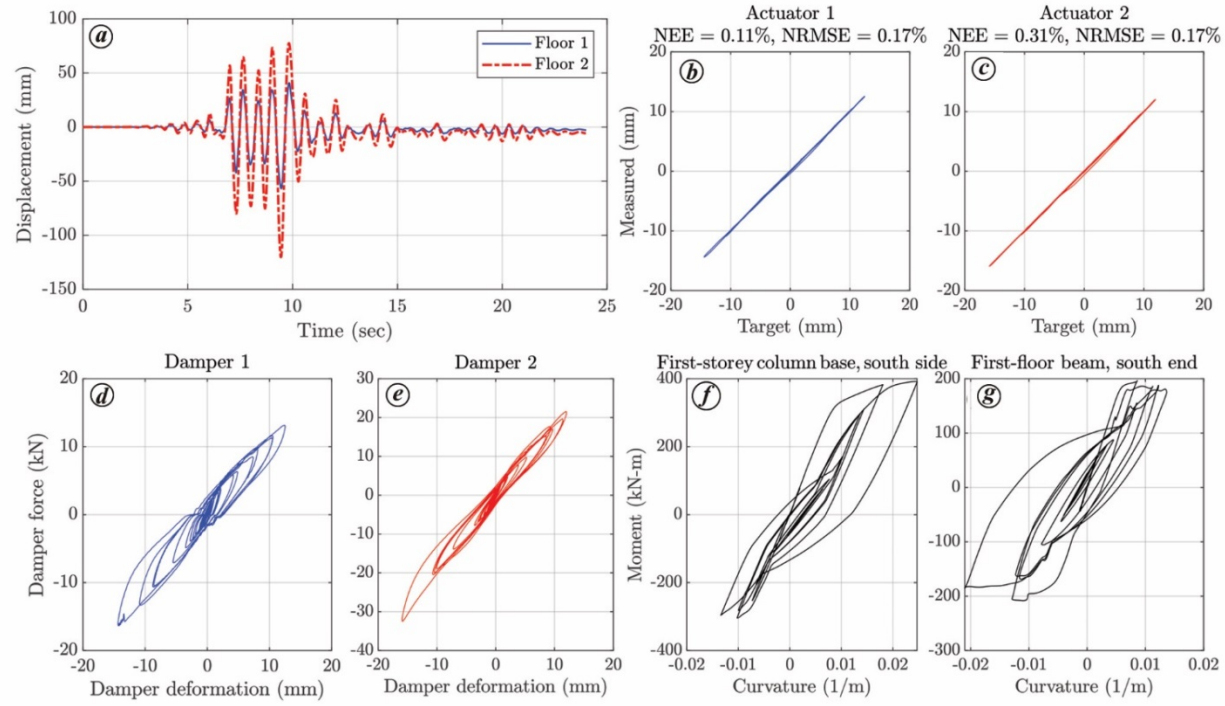

Figure 8. RTHS of two-storey RC-MRF: ***a***, Time history of floor displacements. ***b***, ***c***, Synchronization subspace plots for actuators 1 and 2 respectively. ***d***, ***e***, Force–deformation for dampers 1 and 2. ***f***, ***g***, Moment–curvature response for one column and one beam respectively.

varies between 0 and 1. A value of $\rho_\infty = 1$ implies no numerical damping, whereas $\rho_\infty = 0$ implies asymptotic annihilation (i.e. 100% equivalent damping in the high-frequency limit). In all the RTHS discussed so far, $(\rho_\infty)^2 = 0.25$ was used, which was decided based on a few trial RTHS. For the same equivalent damping in the high-frequency limit, the user-defined parameters of the KR-α and MKR-α methods are related as follows: $\rho_\infty^{\mathrm{KR}} = (\rho_\infty^{\mathrm{MKR}})^2$. Therefore, we prefer to report the value of $(\rho_\infty)^2$ instead of ρ_∞ for the MKR-α method. To demonstrate the essence of numerical damping, RTHS #4 was repeated with $(\rho_\infty)^2 = 0.50$ (i.e. a smaller numerical damping). Figure 7 shows a comparison of the target signal obtained from RTHS #4 and RTHS #6 (Table 1). The result demonstrates the efficacy of controllable numerical damping in eliminating spurious high-frequency oscillations from the target signal.

Finally, to demonstrate the numerical advantages associated with an RTHS, a more detailed nonlinear finite element model of the analytical substructure was developed in HybridFEM-MH, as discussed earlier. An RTHS #7 (Table 1) was then performed for the two-storey RC-SMRF subjected to the same ground motion but scaled to the DBE level. Figure 8 presents both system-level and component-level responses obtained from this test. The floor displacements (Figure 8 *a*) are presented for the former. For the latter, damper force–deformation hysteresis (Figure 8 *d* and *e*) and the moment–curvature section responses in the first-storey south-side column base (Figure 8 *f*) and south end of the first-floor beam (Figure 8 *g*) are presented. The synchronization subspace plots between the target and measured actuator displacements for both actuators are also presented (Figure 8 *b* and *c*) to show the excellent actuator control achieved during the simulation.

In this study, an RTHS framework has been developed at PDTF, IITK. The need for accurate actuator control and controllable numerical damping in performing accurate RTHS is demonstrated using a two-storey RC-SMRF building fitted with nonlinear viscoelastic dampers. A modified procedure is proposed for calculating the ATS parameters a_0 and a_1 when the parameter a_2 reaches its limiting value. Finally, the essence of RTHS in combining the benefits of physical testing with those of advanced computational simulations is demonstrated using a nonlinear analytical substructure. The results show that excellent actuator control can be achieved, and accurate RTHS of structural systems can be performed at the PDTF, IITK.

The information presented here will be useful for implementing the RTHS technique in other laboratories and promoting experimental earthquake engineering research at the national level.

1. Rai, D. C., Jain, S. K., Murty, C. V. R. and Bansal, D., Large capacity reaction floor–wall assembly for pseudo-dynamic testing at IIT Kanpur and its load rating. *Curr. Sci*., 2014, **106**(1), 93–100.
2. Sharma, R., Pseudo-dynamic test on medium-scaled models of steel braces and frames with hysteretic dampers, M.Tech. thesis, Indian Institute of Technology, Kanpur, 2011.
3. Sharma, R., Sachan, A. and Rai, D. C., Correlation between pseudo-dynamic and shake table test on steel truss moment frames with hysteretic dampers. In 15th World Conference on Earthquake Engineering, Lisbon, Portugal, 2012.
4. Kolay, C. and Ricles, J. M., Force-based frame element implementation for real-time hybrid simulation using explicit direct integration algorithms. *J. Struct. Eng.*, 2018, **144**(2), 1–13; doi:10.1061/(ASCE)ST.1943-541X.0001944.
5. Kolay, C. and Ricles, J. M., Improved explicit integration algorithms for structural dynamic analysis with unconditional stability and controllable numerical dissipation. *J. Earthq. Eng*., 2017, **23**(5), 771–792; doi:10.1080/13632469.2017.1326423.
6. Kolay, C. and Ricles, J. M., Development of a family of unconditionally stable explicit direct integration algorithms with controllable numerical energy dissipation. *Earthq. Eng. Struct. Dyn*., 2014, **43**(9), 1361–1380; doi:10.1002/eqe.2401.
7. Kolay, C., Ricles, J. M., Marullo, T. M., Mahvashmohammadi, A. and Sause, R., Implementation and application of the unconditionally stable explicit parametrically dissipative KR-alpha method for real-time hybrid simulation. *Earthq. Eng. Struct. Dyn*., 2015, **44**, 735–755; doi:10.1002/eqe.2484.
8. Kolay, C., Ricles, J. M., Marullo, T. M., Al-Subaihawi, S. and Quiel, S. E., Computational challenges in real-time hybrid simulation of tall buildings under multiple natural hazards. *Key Eng. Mater*., 2018, **763**, 566–575; doi:10.4028/www.scientific.net/kem.763.566.
9. Kolay, C., Al-Subaihawi, S., Marullo, T. M., Ricles, J. M. and Quiel, S. E., Multi-hazard real-time hybrid simulation of a tall building with damped outriggers. *Int. J. Lifecycle Perform. Eng.*, 2020, **4**(1/2/3), 103–132.
10. Kolay, C., Marullo, T. M. and Ricles, J. M., HybridFEM-MH: a program for nonlinear dynamic analysis and real-time hybrid simulation of civil infrastructure systems subject to multi-hazards. ATLSS Report No. 18-06, Lehigh University, Bethlehem, PA, 2018.
11. MATLAB, version 9.8 (R2020a), The Mathworks Inc., Natick, MA, USA, 2020; https://in.mathworks.com
12. Simulink Real Time. The Mathworks Inc., Natick, MA, USA; https://in.mathworks.com/products/simulink-real-time (accessed on 26 May 2022).
13. ASCE/SEI 7-16, Minimum design loads and associated criteria for buildings and other structures, American Society of Civil Engineers, USA, 2017; doi:10.1061/9780784414248.
14. Chae, Y., Kazemibidokhti, K. and Ricles, J. M., Adaptive time series compensator for delay compensation of servo-hydraulic actuator systems for real-time hybrid simulation. *Earthq. Eng. Struct. Dyn*., 2013, **42**, 1697–1715; doi:10.1002/eqe.2294.
15. Kolay, C., Parametrically dissipative explicit direct integration algorithms for computational and experimental structural dynamics. Department of Civil and Environmental Engineering, Lehigh University, Pennsylvania, USA, 2016.

ACKNOWLEDGEMENTS. We thank Science and Engineering Research Board, Government of India (ECR/2018/001997) and the Indian Institute of Technology Kanpur (IITK), for providing financial support during this study. Avadh Rail Infra Ltd donated the raw materials (viz. Indian natural rubber and other chemicals) required to manufacture the viscoelastic dampers used in the study. We also thank Mohit Dwivedi (Structural Engineering Laboratory, IITK) for help in performing the real-time hybrid simulations. Any opinions, findings and conclusions expressed in this communication are those of the authors and do not necessarily reflect the views of the sponsors.

Received 12 March 2023; re-revised accepted 25 July 2023

doi: 10.18520/cs/v125/i6/685-691